Polar Meteorol. Glaciol., **16**, 116–132, 2002

In-situ ice and meteorological observations in the southern Sea of Okhotsk in 2001 winter: ice structure, snow on ice, surface temperature, and optical environments

Takenobu Toyota[1], Kenji Baba[2], Eisuke Hashiya[3] and Kay I. Ohshima[1]

[1] *Institute of Low Temperature Science, Hokkaido University, Sapporo 060-0819*
[2] *Graduate School of Environmental Earth Science, Hokkaido University, Sapporo 060-0810*
[3] *Weathernews Inc., Nakase 1-3, Mihama-ku, Chiba 261-0023*

Abstract: The 2001-ice season in the Sea of Okhotsk was characterized by extraordinarily developed ice extent. During the period February 17 to 21, we conducted *in-situ* observations in the southern ice area with the icebreaker '*Soya*'. In this paper, we show the observational results, concerning the core sampling of about 1.3 m-thick ice, snow sampling, surface temperature, and solar radiation under clear sky conditions. It is shown that (1) the sampled ice core is composed entirely of granular ice, (2) the 30 cm-thick snow pack overlying sea ice is composed mainly of depth hoar and significant vertical gradients of $\delta^{18}O$ and temperature are found within the snow, probably associated with the depth hoar formation, (3) surface temperatures as low as about -30℃ are detected on snow-covered sea ice floes at nighttime under almost clear and light breeze conditions, (4) from the estimation of the turbidity coefficient, the atmosphere over the ice-covered area is considered to be significantly clean. Furthermore, the NOAA/AVHRR satellite data are used to estimate the surface temperature distribution in the southern Sea of Okhotsk. It is shown that these data are useful for discriminating thick ice floes.

1. Introduction

The 2001 sea ice season in the Sea of Okhotsk was characterized by the extraordinarily large extent of sea ice (Fig. 1a). The sea ice extent reached its maximum on March 5, occupying 97% of the whole Sea of Okhotsk. The maximum sea ice area amounted to 151.67×10^4 km^2, the second largest on record next to 152.25×10^4 km^2 in 1978 (Kaneko *et al*., 2002). Since the average value from 1971 to 2000 was 122.83×10^4 km^2 (s.d.$=14.78\times10^4$ km^2), according to the Japan Meteorological Agency, the maximum ice area in 2001 was larger by as much as 23% than normal. In mid February, during the season of increasing ice extent, we conducted *in-situ* ice, meteorological, and hydrographical observations using the P/V *Soya* in the southern Sea of Okhotsk. Through this cruise observation, we found out that both ice thickness and ice extent were considerable. Our ship needed to repeatedly charge the ice to advance (the ice breaking ability of the ship is 1.2 m) and was often forced to take thinner routes. Eventually, we had to give up our observations and return, having completed only half of our planned course (Fig. 1b). According to the statistics of ice thickness that we

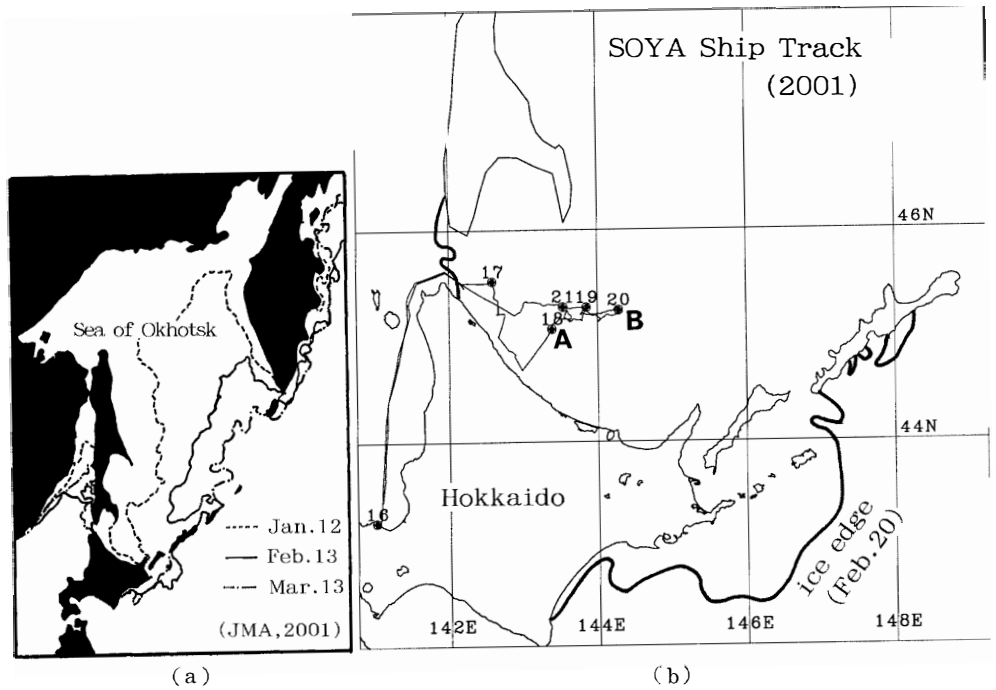

Fig. 1. Sea ice extent in the Sea of Okhotsk in winter 2001:
(a) for the whole Sea of Okhotsk,
(b) for the southern Sea of Okhotsk with the ship tracks (thin lines) and the ice edges (thick lines) on February 20, 2001.
The number and circular marks in the figure denote the date and ship positions at noon, respectively. Points A and B denote the sampling points of an ice core and snow, respectively.

measured in the same region from 1996 to 2000, the averaged ice thickness ranges from 20 to 55 cm, and ramming(*) was seldom needed during the cruises.

Although we were prevented from completing our observation cruise by thick ice, this developed sea ice enabled us to get off of the ship and take ice core samples of more than 1 m thickness on sea ice with an ice auger, the first time we have done so in this region. We examined profiles of textural structure, density, salinity, and $\delta^{18}O$. Along with ice sampling, we also examined the characteristics of the snow overlying sea ice. Recently the attention paid to the characteristics of snow on sea ice has been increasing because it substantially controls the heat exchange among atmosphere, ice, and ocean in the sea ice region due to its low thermal conductivity and high albedo. However, the observations of snow on sea ice are still limited, especially in the seasonal ice zone. While there has been some research done, particularly in the Antarctic (*e.g.* Sturm *et al.*, 1998; Morris and Jeffries, 2001), few studies have been done in the Sea of Okhotsk. Therefore, we here report our result concerning the snow observations.

As a first trial in the interior pack ice region in the Sea of Okhotsk, the surface

(*) Ramming is to go backward once and charge ice with great force when it is difficult for a ship to proceed in the ice area, prevented by remarkably thick ice.

temperatures were monitored during the cruise with a downward-looking infrared thermometer at the ship's bow. From the thermodynamical viewpoint, the surface temperature of sea ice is one of the most important factors. It is directly related to heat exchange between sea ice and atmosphere and thereby determines the ice growth amount. However, the direct measurement of surface temperature has been very limited, especially in the seasonal ice zones, because of the observational difficulty. Here we show the observational result, paying attention to the difference from the air temperatures measured at altitude 15 and 19 m above sea level. Furthermore, the surface temperature distribution is also estimated from NOAA/AVHRR satellite data to examine the two dimensional distribution in addition to the linear measurement along the cruise track.

In the growth of sea ice in the southern Sea of Okhotsk, which is located at relatively low latitude, solar radiation plays a crucial role (Toyota and Wakatsuchi, 2001) and there is a need for accurate prediction of solar radiation. However, there is a problem in that multiple reflections between surface and cloud base contribute a substantial amount of downward radiation over high albedo surfaces (Shine, 1984). To precisely estimate the cloud effect, measurement under cloudless conditions seems to be requisite. Fortunately, we came across a clear sky during the daytime on February 20. Besides, the ship position was restricted around N 45.24° E 144.28° because our navigation was prevented by unusually thick ice floes. This situation allowed us to obtain surface solar radiation data at an almost fixed position under the same ice conditions, not hindered by cloud. Using these solar radiation data, we verify the formula derived by Shine (1984) and furthermore estimate the atmospheric turbidity in this ice area.

Thus, the purpose of this paper is to report the comprehensive results of the above ice and meteorological observations as one *in-situ* record obtained under remarkably large ice-extent conditions for an understanding of the ice growth process in the seasonal ice zones.

2. Observations

The observations were conducted during the period 17–21 February in the southern Sea of Okhotsk. The cruise track is shown in Fig. 1b. In the observations, ice thickness, air temperature, relative humidity, surface temperature, wind, upward and downward short wave radiation were monitored. Ice thickness was estimated from the images monitored by a downward looking video camera (Fig. 2a). On the images, we measured the thicknesses of individual ice floes which turned into side-up positions (see Toyota *et al.* (1999) for details.). The distribution of 10-min averaged ice thickness is mapped in Fig. 2b. Since the ship took the thinner route this year, this map is biased to thinner ice. Even so, at several points averaged ice thickness exceeded one meter. Such a thick ice area has not been detected since 1991 when these measurements were started. Around these thick ice regions, we succeeded in taking an ice core sample with an ice auger.

Air temperature and relative humidity were measured every minute at the ship mast at heights of 14.7 m and 19.0 m above sea level. Wind was measured every minute with

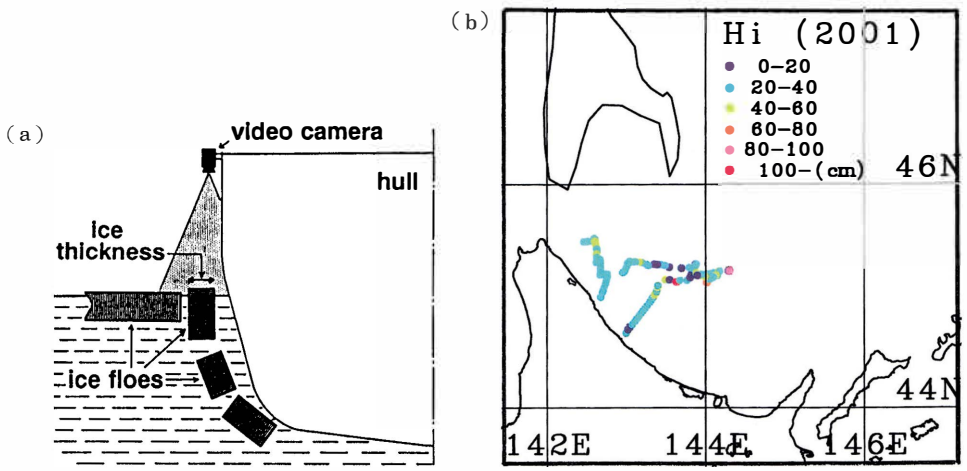

Fig. 2. Ice thickness measurement by video monitoring.
(a) Schematic picture of observation (cited from Shimoda et al., 1997).
(b) Ice thickness distribution. Ice thickness was calculated by averaging the individual thicknesses, measured as in Fig. 2a, for 10 min.

an anemometer at the upper deck at the height of 14.0 m above sea level. The real wind was calculated by subtracting the ship's velocity from the raw anemometer data. Upward and downward short wave radiations were measured every minute with pyranometers of the S-185 type, which was designed for measurement on ships by Ishikawa Sangyou KK. They measure short wave radiation in the wavelength region 300–2800 nm from omni directions within a hemisphere with the accuracy of $\pm 2\%$, using a thermopile. Their surfaces were kept horizontal by a gimbaling mechanism (see Toyota *et al.* (1999) for details.). Surface temperature was measured every minute with a HORIBA IT-340W downward-looking infrared thermometer at the ship's bow. The measurement wavelength is from 8 to 12 μm and the accuracy is $\pm 0.5^{\circ}$C. The sight range is estimated as a 1.5 m-diameter circle on the surface beneath the instrument, and thus the obtained data seem to be free from the effect of the ship's body. Since the emissivity of the snow-pack is around 0.98 for the long wavelength of 4–11 μm (Berger, 1979), which is close to 1, the unit value is used here.

3. Results

3.1. Ice structure

We carried out ice core boring on February 18 and 20. The core obtained on February 20 was broken into pieces when it was taken out from the core barrel and could not be analyzed. Therefore only the result of the one taken on February 18, amounting to 130 cm in length, is shown here. The sampling point is shown as A in Fig. 1b. The core sample is shown in Fig. 3a. The core is composed of several pieces, suggesting that this ice floe was formed by accumulation of several ice floes. Vertical profiles of textural structure, salinity, density, and δ^{18}O were examined. Figure 3b shows the core analysis method. First, the core was cut into halves, and then each part

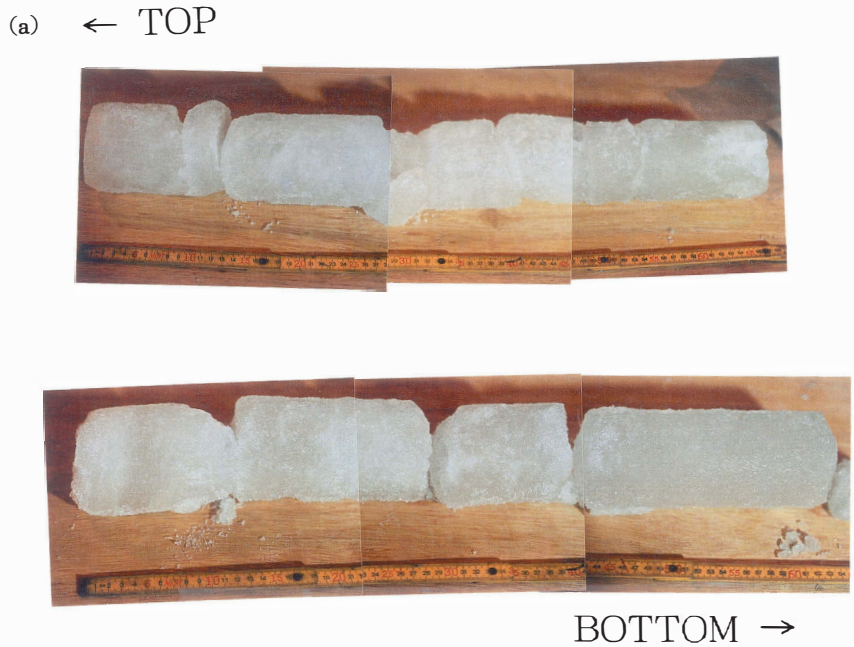

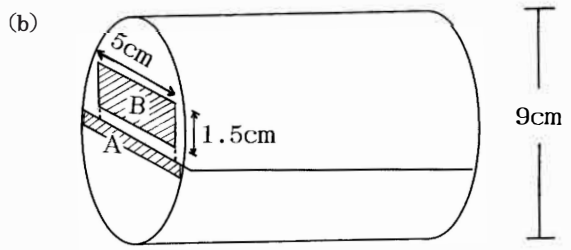

Fig. 3. The ice core sample collected at Point A (Fig. 1b) with an ice auger on sea ice.
(a) Photograph of the sample (the upper left is at top, and the lower right is at bottom).
(b) A schematic illustration of core analysis. a was used for thin section analysis and b for the measurement of density, salinity, and $\delta^{18}O$.

was used for thin section analysis (A) and analysis of physical and chemical properties (B), respectively. Through thin section analysis using a microtome the textural structure was examined. For measurement of physical and chemical properties, rectangular ice sections were made at intervals of 3–4 cm from column B in Fig. 3b. Density was estimated by measuring the three dimensions of the ice section (refer to Fig. 3b) and its weight. After the samples were melted at room temperature, salinity was measured with a salinometer (Towa Electronic Industry, Model SAT-210) with an estimated precision of <0.05 psu. In addition, $\delta^{18}O$ was measured with a mass spectrometer (Delta plus) with an estimated accuracy of 0.023.

The results are shown in Fig. 4a–4d. In Fig. 4a, both photographs of thick (5 mm) and thin (<1 mm) ice sections are shown. The former depicts the distribution of

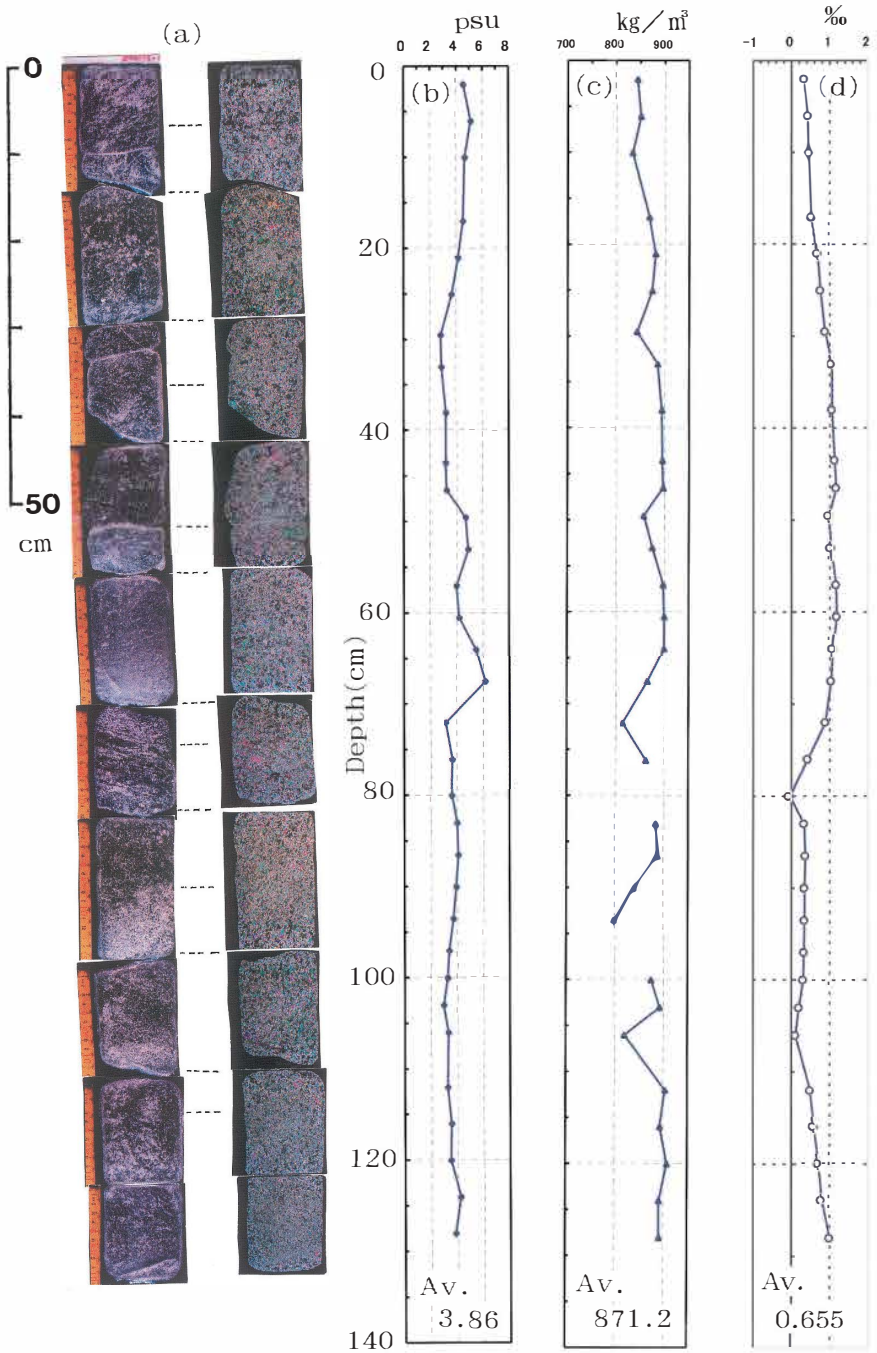

Fig. 4. The vertical profiles of the ice core.
(a) Right: Polarized photograph of thin section (<0.5 mm).
Left: Photograph of thick section (5 mm).
(b) Ice salinity. (c) Ice density. (d) $\delta^{18}O$.

inclusions in the ice, while the latter shows the crystal arrangement. From these photos, the layered structure can be seen, though it is not very clear. The possible boundaries, which are determined from different pieces of the ice core and the difference of inclusions or crystal size and arrangement, are drawn with broken lines in the figure. Some variations are also seen in the profiles of salinity, density, and $\delta^{18}O$ (Fig. 4b–4d). Some of them match with the broken lines in Fig. 4a. These results suggest that this sea ice floe is composed of several ice layers. The averaged layer thickness is estimated to be 8.7 cm from Fig. 4a. In addition, it is noticeable in Fig. 4a that the sample is composed entirely of granular ice. This indicates that a turbulent dynamical process was dominant rather than thermodynamical bottom freezing during the ice formation. Takizawa *et al.* (1987), through the analysis of the 56 cm-thick ice collected on a sea ice floe off Mombetsu, showed that granular ice occupies about half of the thickness and the ice sample is composed of several layers. Ukita *et al.* (2000), through the analysis of young ice samples collected in 1996, showed that they are composed of granular ice and have a layered structure. Toyota *et al.* (2001a), from the ice samples collected from 1996 to 2000, also showed statistically that a granular structure occupies 74% of the total thickness and the averaged layer thickness is 8.1 cm. As shown from these results, the ice growth processes under turbulent conditions, such as frazil ice accumulation and rafting, are dominant in the southern Sea of Okhotsk. Our observations showed that these characteristics could be found in developed ice more than 1-m thick. Although columnar ice was detected in the young ice collected at other points during this cruise, granular ice is a major ice type in this area. These features are similar to those of sea ice in the Antarctic (*e.g.* Lange and Eicken, 1991; Worby *et al.*, 1996).

The averaged density (871.2 kg/m^3) is lower than the value of 920 kg/m^3 estimated for the first-year ice in the polar region by Tucker *et al.* (1991) and rather closer to the value of 887$\pm$20 kg/m^3 estimated for the multi-year ice by Eicken *et al.* (1995). The averaged salinity (3.86 psu) is about 2 psu lower than that of the first-year ice of the same thickness in the polar region (refer to Cox and Weeks, 1974). and also rather closer to that of multi-year ice. As pointed out from the surface heat budget by Toyota *et al.* (2000), surface melting and the subsequent flushing process may be responsible for these low values. It is shown from the $\delta^{18}O$ profile that almost all the data have positive values. Considering that negative $\delta^{18}O$ can be an indicator of snow ice for the southern Sea of Okhotsk (Toyota *et al.*, 2001b), this thick ice core seems to have originated from sea-water and the contribution of snow is small although the snow on the ice was unusually thick (more than tens of centimeters). All these data are consistent with the characteristics found of ice samples collected from 1996 to 2000 in the southern Sea of Okhotsk.

3.2. Snow on sea ice

We examined the snow characteristics on a sea ice floe at point B in Fig. 1b on February 20. The ice thickness was estimated as more than 2 m from ice drilling and the snow depth was 30 cm. The snow type was depth hoar over the whole depth and the grain size was 0.5 to 1.0 mm (Table 1). Temperature was measured with a thermistor thermometer at intervals of 10 cm. In addition, snow was sampled with a snow sampler (5.5 (W) $\times$ 6.0 (D) $\times$ 3.0 (H) cm) at intervals of 10 cm, and its salinity and

Table 1. Observational results of snow properties on sea ice.

Date	Time (JST)	Temp. (°C)	Snow depth (cm)	Snow type	Grain size (mm)	Salinity (‰)	$\delta^{18}O$ (‰)
2001/2/18	7:24			new	0.1–0.2	0.15	−14.762
	7:35	−3.2	12	new	0.1–0.2	0.34	−14.951
	10:20	−3.8	10	new	0.2	1.28	−15.389
	13:50	−4.3	15	new	0.2	0.11	−17.979
	23:25					0.26	−17.568
2001/2/19	7:40	−18.0	20	new	0.2	0.07	−17.845
	13:35	−8.1	5	new	0.2	0.09	−18.091
	15:30	−9.2	10	new, depth hoar	0.5–2	1.66	−16.692
2001/2/20	6:45	−16.3	15	new	0.2	0.12	−19.218
	10:15	−5.6	30 (0)	depth hoar	0.5–1	0.19	−12.228
		−7.2	30 (10)	depth hoar	0.5–1	0.07	−14.746
		−9.5	30 (20)	depth hoar	0.5–1	0.05	−16.781
		−10.3	30 (30)	depth hoar	0.5–1	<0.05	−17.891
	10:30			depth hoar	0.5–1	0.07	−17.582
2001/2/21	8:05	−7.0	5	depth hoar	0.5–1	1.19	−17.839
	13:50	−1.7	18	depth hoar	0.3–0.5	0.05	−14.931

The hatched samples were taken on sea ice at point *B* (Fig. 1b).
The parenthesized figures denote the level from the snow-ice interface in cm.
The other samples were taken from the ship with a ladle.

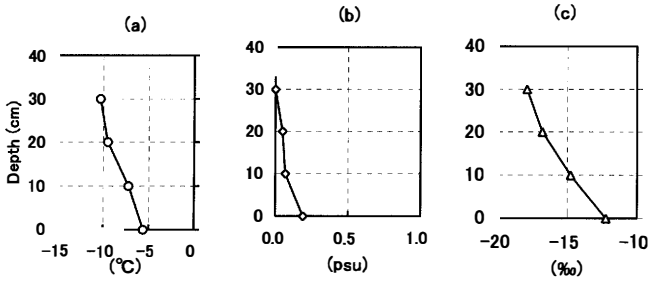

Fig. 5. The vertical profiles of the 30 cm-thick snow overlying sea ice. The 0 cm-depth corresponds to the snow-ice interface. (a) Temperature. (b) Salinity. (c) $\delta^{18}O$.

isotopic composition were measured after it was melted at room temperature. Figure 5a–5c show the vertical profiles of temperature, salinity and $\delta^{18}O$. In these figures, significant vertical gradients are found for temperature and $\delta^{18}O$. On the other hand, for salinity the value is small and the vertical gradient is relatively small, indicating that the snow pack was only slightly affected by seawater.

From these results, the following scenario is inferred: first a strong vertical temperature gradient is produced due to surface cooling, and accordingly a vertical gradient of vapor pressure develops if vapor pressure is locally saturated within the snow

layer. Then the vapor pressure gradient induces upward vapor flux. To maintain the vapor-saturated conditions, sublimation occurs at each level and then the $\delta^{18}O$ increases at the bottom layer and decreases at the surface layer. Consequently, a vertical gradient of $\delta^{18}O$ is observed within the snow layer. During this process, depth hoar develops through repeated sublimation.

This process is common for the snow pack, especially near the surface with a strong vertical temperature gradient, and there has been a great deal of research on snow on the ground (*e.g.* Hachikubo *et al.*, 2000). However, there have been few reports for snow on sea ice. In the case of relatively thin sea ice, the vertical temperature gradient within the overlying snow tends to be strong because the snow depth is restricted due to the isostasy balance and the temperature at the bottom is maintained at a relatively high temperature affected by underlying warm sea-water. Therefore it is considered that depth hoar develops easily and is one feature of the snow overlying sea ice. During the cruise, we collected snow samples with a ladle from the ship at several points. Because the bulk snow pack was sampled, the vertical profiles of the snow properties could not be obtained at these points. The snow depth was measured with a snow depth gauge from the ship. Table 1 lists all the results obtained. It is found in this table that depth hoar is relatively common, together with new snow. According to the results for the west Antarctic pack ice reported by Sturm *et al.* (1998), depth hoar occupies 30 to 50% and is the dominant snow type. These results support our speculation. It may be possible that the vertical gradient of $\delta^{18}O$ at point B is caused by the variation of snowfall $\delta^{18}O$. However, considering that $\delta^{18}O$ ranges between -15 and -19 ‰ at other points, it is natural that a value as high as -12 ‰ at the bottom layer at point B is caused by sublimation. According to Hachikubo *et al.* (2000), the $\delta^{18}O$ of the snow near the surface can decrease by about 2 ‰ for one night. Thus the observed value is attributed to sublimation.

3.3. Surface temperature

Figure 6a shows the time series of surface temperature (T_s) during the cruise, along with air temperature data. The large fluctuation of T_s with a short period was caused by repeated ship ramming. When the ship moved forward the thermometer measured surface temperatures of sea ice, while higher temperatures were recorded in the open water when the ship moved backward. Therefore, the lower envelope of the graph probably represents the ice surface temperature. As mentioned in the previous section, snow samples were picked up at 10 points during the cruise, and the temperatures were directly measured for validation. The data are plotted with triangles in Fig. 6a. Although the data cannot be compared directly with T_s, both values almost coincide within about 1°C.

In Fig. 6a, temperatures as low as about -30°C were observed from 19 h to 23 h on February 19. At this time, air temperature was around -15°C at 14.7 m height, suggesting that a strong inversion was formed near the surface layer. The temperature time series during this period is shown in more detail in Fig. 6b with air temperatures at two levels. The temperature difference between the surface and 19.0 m height amounted to as large as 15–20°C, from which the vertical temperature gradient is estimated as about 1°C/m. At this time, wind speed was relatively weak, averaging 2.0

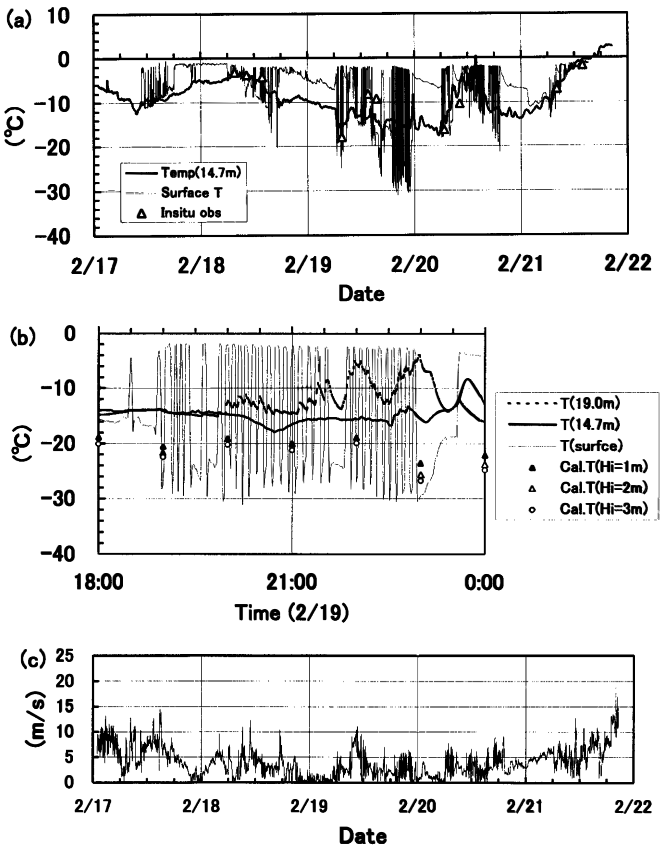

Fig. 6. Surface temperature data monitored by an infrared thermometer.
(a) Time series during the cruise with air temperature at 14.7 m (thick line) and in-situ measurement of snow (triangle).
(b) Close-up of (a) for the period from 18 h to 24 h on February 19, with air temperature at 19.0 m height (broken thin line).
The surface temperatures calculated from a one-dimensional thermodynamical model are also plotted (triangle) for 1, 2, and 3 m thick ice.
(c) Time series of wind speed data during the cruise.

m/s from 18 h to 24 h (Fig. 6c). Although the exact ice thickness was unknown because of darkness, the thickness seems to be much more than 1 m, considering that the ship needed repeated ramming to proceed.

We could not reproduce this low surface temperature from the one-dimensional thermodynamical ice model which assumes that all the heat fluxes are balanced at the surface. The values calculated for Hi＝1, 2, 3 m using this model are also plotted in Fig. 6b (See Toyota *et al.* (2000) for the detailed method of calculation). Possible reasons include the imbalance of heat fluxes at the surface and the uncertainty of downward long wave radiation. We need to investigate this imbalance through precise measurements.

To examine the two dimensional distribution of surface temperature in addition to

the one dimensional measurement along the cruise track, the NOAA/AVHRR ch4 and ch5 data on 1513 of February 19 are used. In the calculation of surface temperature, the following formula is applied (TeraScan 2.6 Reference Manual, 1995).

$$SST = 1.017342 \times Ch.4 + 2.139588 \times (Ch.4 - Ch.5) + 0.779706 \times (Ch.4 - Ch.5) \times (\sec(sza) - 1) - 0.543,$$

where *Ch.4* and *Ch.5* are the brightness temperatures of channels 4 and 5, respectively, and *sza* is the zenith angle of satellite NOAA. Figure 7b shows the distribution of surface temperature calculated at each pixel with the cruise track on February 19. To distinguish from cloud, a visible image of AVHRR (ch1) is also shown (Fig. 7a). The calculated area is scarcely affected by cloud and seems to represent the ice surface temperature.

Although the satellite data cannot be compared directly with the *in-situ* data, the local minimum of -24.5℃ at 1601 around the satellite scan time is nearly equal to the satellite-derived temperature (N 45.22°, E 144.10°). In this figure ice floes with significantly low surface temperature can be clearly distinguished in the analyzed area, probably corresponding to remarkably thick ice (refer to blue-colored areas, corresponding to below -20℃, in the figure.). Because the ship selected a thinner ice route as suggested from the cruise track in Fig. 7b, we cannot know the exact ice thickness of

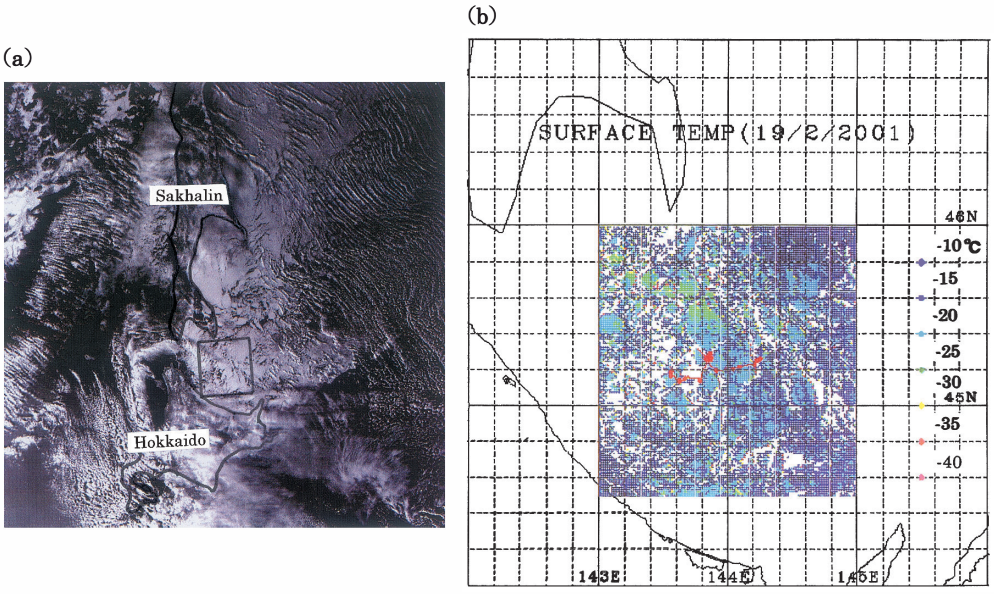

Fig. 7. NOAA/AVHRR image at 1513 (JST) on February 19, 2001.

(a) Visible image (Ch. 1). This picture shows the cloud cover distribution. The coastlines of Hokkaido and Sakhalin are depicted. The square area corresponds to the colored region in Fig. 7b.

(b) Surface temperature distribution derived from Ch. 4 and Ch. 5 with the cruise track (red line) on Feb. 19.
The white portion within the colored area corresponds to $T_s > -10$℃.

the thick ice floes. However, considering that our ship sometimes needed to repeat ramming on this day, the ice thickness is estimated to be much more than 1 m. Many floes have diameters of more than 10 km and are distributed in patches. This feature cannot be detected only from the visible image; this result suggests that surface temperature is useful for the detection of thick ice floes.

3.4. Optical environments

As suggested in the daily variation of solar radiation of Fig. 8a, February 20 was a completely clear day without cloud during the daytime except for very early hours.

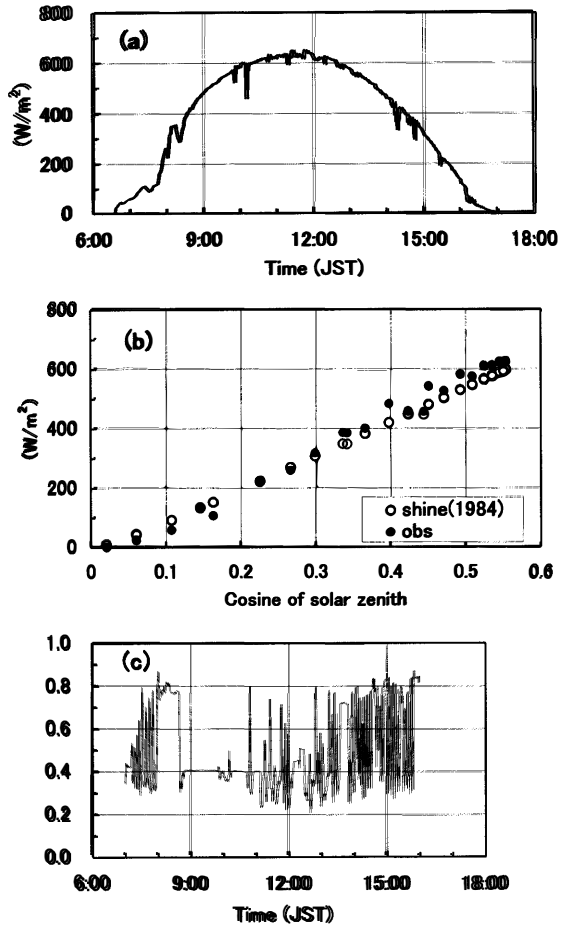

Fig. 8. Surface solar radiation data on February 20, 2001.
(a) Daily variation of incident solar radiation.
(b) Comparison with the calculation by Shine (1984) as a function of the cosine of solar zenith.
(c) Daily variation of albedo. In this figure, the large fluctuation was caused by repeated ramming.

Using these data, the optical environments of the atmosphere in this region are examined. Shine (1984) derived the surface solar radiation flux formula as follows:

$$S_{\mathrm{cal}}=S_0\mu^2/(1.2\mu+(1.0+\mu)e_a\,10^{-3}+0.0455), \qquad (\mathrm{W/m^2})$$

where S_0, μ, and e_a are the solar constant, the cosine of solar zenith and the surface water vapor pressure in hPa, respectively. This is a modified version of the formula given by Zillman (1972) and was introduced to include the effect of multiple reflections due to clouds for high albedo surfaces. We verify this formula with our data. In Fig. 8b, the observed data and the calculated values from the above formula are plotted at intervals of 30 min as a function of the cosine of solar zenith. The observed values are larger by 20–30 W/m^2 (about 6% on average) than the calculated values. We consider that this discrepancy is caused by the effects of multiple reflections (due to Rayleigh scattering, not clouds) and the presence of aerosols, which are neglected in the above formula. Shine (1984) pointed out that multiple reflections cause a maximum error of about 5%, which almost coincides with our result (about 6%). For convenience, the following regression of solar radiation from the cosine of solar zenith is obtained from our observations (Fig. 8b):

$$S=1260.6\mu-57.5, \qquad (\mathrm{W/m^2})$$

where S is the observed surface solar radiation under a clear sky.

Next we examine the effect of aerosols. For this, we estimate the atmospheric turbidity in this area by comparing the incident surface solar radiation data with the theoretically predicted solar radiation at the top of the atmosphere. For atmospheric turbidity, Linke's turbidity factor (1942) and the turbidity coefficient of Ångström (1961) have usually been used. The former represents the degree of reduction of solar radiation along the atmospheric path. Although this is a simple and useful formulation calculated from routine observations, we cannot discriminate the individual effects of vapor, aerosol, and selective absorption by gaseous constituents (O_3, and CO_2). On the other hand, the latter can detect the effect of aerosols. However, this method requires measurements of direct solar radiation with use of filters and cannot be applied here. In this study, we use the turbidity coefficient (β) developed by Yamamoto *et al.* (1968). This method was introduced to estimate the turbidity coefficient from direct solar radiation measurements without using filters under the assumption that the size distribution of aerosols obeys the Junge distribution. Yamamoto *et al.* (1968) estimated the turbidity coefficient over a widespread area in the northern hemisphere using direct solar radiation data measured during the IGY, and mapped the distribution of β for each season. Here we compare the turbidity coefficient obtained from our observations with their results for winter, and examine the aerosol environment in the southern Sea of Okhotsk.

Since we measured global solar radiation (not direct solar radiation), we needed to use the following transformed formula described by Kondo (2000).

$$\begin{aligned} S=S_0\times&(0.21-0.2\beta+0.7\times10^{-M(0.056+0.16\sqrt{\beta})})\\ &\times(1-0.014\times(M+7+2\times\ln(w^*/10))\times\ln(w^*/10))\\ &\times(1+(0.066+0.34\sqrt{\beta}\,)\times(\alpha-0.15)), \end{aligned}$$

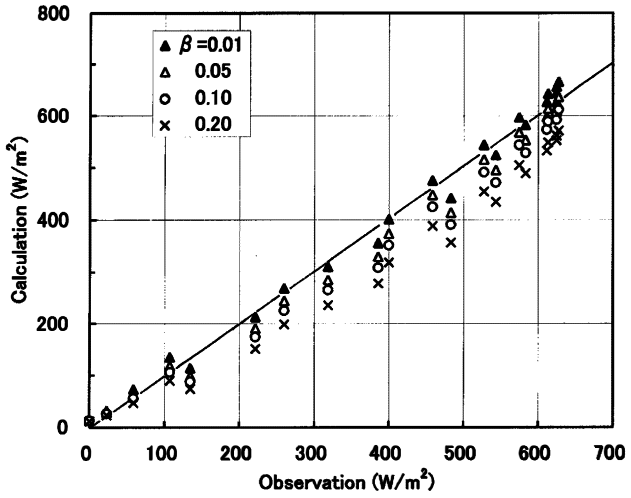

Fig. 9. Dependence of surface solar radiation on turbidity coefficient (β) defined by Yamamoto et al. (1968). Vertical and horizontal axes are observed and calculated values, respectively. See the text for the method of calculation.

Table 2. Root-mean-square of the difference between observation and calculation of solar radiation for various β. Refer to Fig. 9.

β	RMS (W/m^2)
0.01	21.4
0.02	**20.6** (Optimum value)
0.03	22.0
0.04	24.4
0.05	27.3
0.10	42.9

where α and w^* are the surface albedo and the precipitable water, respectively. M is the atmospheric optical path and defined as $(p_0/1013.2)/\mu$, where p_0 is surface pressure in hPa. For α, the value of 0.8 used here is from our *in-situ* observations (Fig. 8c). In the figure, large fluctuation is caused by repeated ship ramming and thus the real albedo seems to be the upper envelope of the variation. To obtain w^*, we examined the relationship between the surface vapor pressure (e_a) and the precipitable water from the radiosonde observations which were carried out on board *Soya* in the Sea of Okhotsk from 1998 to 2000, and found that both data have good correlation ($r=0.73$). The regression, $w^*=1.396\,e_a-0.356$, is used to estimate w^* from the observed e_a.

On the basis of the above formula, we determined the optimum value of β which minimizes the RMS between the observation data and the calculated values. As a result, we found that β is estimated as 0.02 (Fig. 9, Table 2). Although α appears to have some variations from 0.70 to 0.80 in Fig. 8c, the sensitivity of the optimum β to albedo is found to be small. Compared with the map depicted by Yamamoto *et al.* (1968) in their Fig. 19, this value corresponds to the lower limit (*e.g.* $\beta=0.147$ for Tokyo, 0.090 for Sapporo, 0.065 for Washington), and, interestingly, is equal to the

value at Okhotsk City located on the northern coast of the Sea of Okhotsk. It is suggested from this result that the atmosphere is particularly clean in the observation area.

4. Summary and discussion

In the 2001 ice season, characterized by the extraordinarily large extent of sea ice in the Sea of Okhotsk, we conducted ice and meteorological observations in the southern region. Among the observational data, we here describe the results which were obtained in the ice area. In the ice pack region, ice core samples were collected with an ice auger and the overlying snow was also sampled. The physical and chemical properties of ice and snow are examined. During the cruise, we monitored the surface temperature with an infrared thermometer at the ship's bow. The vertical profile of temperature near the surface is examined with these data. In addition, on February 20 we came across completely cloudless conditions during the daytime. Using the solar radiation data on this day, the optical environment of the atmosphere in this region is examined.

As a result, the following characteristics were found: (1) the ice core of about 130 cm thickness was composed entirely of granular ice, (2) the $\delta^{18}O$ showed mostly positive values over the whole thickness with some fluctuation, (3) the snow pack of 30 cm thickness overlying sea ice was composed mainly of depth hoar, probably developed due to the strong vertical temperature gradient, (4) a significant vertical gradient of $\delta^{18}O$ was also detected, possibly associated with sublimation, (5) at nighttime under the almost clear sky and light breeze conditions, the surface temperature of snow-covered sea ice floes decreased to about $-30^{\circ}C$, and the vertical gradient of air temperature below 20 m height was about $1^{\circ}C/m$, (6) the surface temperature distribution estimated from satellite data (NOAA/AVHRR ch4 and ch5) outlines thick ice floes with diameters of more than 10 km, (7) the observed surface solar radiation data under clear conditions are by about 6% larger than those calculated from the Shine (1984) formula, and this increase is considered to be caused by the effect of multiple reflections due to Rayleigh scattering, (8) the atmospheric turbidity coefficient (β) defined by Yamamoto *et al.* (1968) is estimated as 0.02, corresponding to the lower limit of the β distribution in winter for the northern hemisphere.

The result (1) suggests that dynamical ice growth processes under turbulent conditions such as frazil ice formation and floe accumulation are dominant for thick ice as well in this region. The result (2) shows that the contribution of snow ice is small and this thick ice floe originated basically from seawater. This suggests that snow ice formation is not essential in this region as Toyota *et al.* (2001b) concluded from 5 years of data. Results (3) and (4) are connected with each other and are typical features related to depth hoar formation. Considering that snow depth on sea ice is relatively restricted due to the isostasy balance, the vertical gradient of temperature within snow tends to be strong, resulting in the promotion of depth hoar formation. As for result (5), we could not reproduce this low surface temperature from a one-dimensional thermodynamical ice model which assumes that all the heat fluxes are balanced at the surface. From result (8), it is suggested that the atmosphere was significantly clean

over this ice-covered area. The turbidity coefficient (β) is the same as the value estimated by Yamamoto *et al.* (1968) for Okhotsk City; this low β may be a characteristic of the optical environment over the ice-covered Sea of Okhotsk. One possibility is that sea ice cover plays a role in suppressing the generation of aerosols of sea water origin, and this effect might be distinct in this remarkable ice year. However, further measurement of solar radiation under various ice conditions will be needed to confirm this effect.

We showed several aspects of sea ice characteristics in the southern Sea of Okhotsk from the observations in 2001. In this paper, we focused on the description of the characteristics in connection with the extraordinarily developed ice conditions. Although the data are limited, some of the results described here could be obtained for the first time due to the developed sea ice. To generalize our results, further observations under various ice conditions will be required.

Acknowledgments

We are sincerely grateful to the crew of P/V *Soya* of the Japan Coast Guard and our colleagues at ILTS for their kind cooperation throughout the cruise. Special thanks are given to co-workers Genta Mizuta and Kenji Nakata, and to Prof. Masaaki Wakatsuchi of ILTS, for support of the observations. We are also indebted to N. Iwasaka of Tokyo University of Mercantile Marine for the pyranometers, to Prof. Hiroyuki Enomoto of Kitami Institute of Technology and Masashige Nakayama of Tokai University for processing the NOAA data, and to Takeshi Nakatsuka of ILTS for the measurement of $\delta^{18}O$. Useful discussions with all the members of the Oceanographic division of ILTS are also acknowledged. This work was partially supported by a fund from the Core Research for Evolutional Science and Technology, Japanese Science and Technology Corporation.

References

Ångström, A.K. (1961): Technique of determining the turbidity of the atmosphere. Tellus, **13**, 214–223.

Berger, R.H. (1979): Snowpack optical properties in the infrared. CRREL Rep., **79-11**, 1–9.

Cox, G.F.N. and Weeks, W.F. (1974): Salinity variations in sea ice. J. Glaciol., **13**, 109–120.

Eicken, H., Lensu, M., Lepparanta, M., Tucker III, W.B., Gow, A.J. and Salmela, O. (1995): Thickness, structure, and properties of level summer multiyear ice in the Eurasian sector of the Arctic Ocean. J. Geophys. Res., **100**, 22697–22710.

Hachikubo, A., Hashimoto, S., Nakawo, M., Motoyama, H., Suzuki, K. and Nishimura, K. (2000): Isotopic mass fractionation of surface snow due to hoarfrost formation. Seppyo (J. Jpn. Soc. Snow Ice), **62**, 265–277 (in Japanese with English abstract).

Kaneko, H., Mori, K. and Matsumoto, T. (2002): Characteristics of sea ice conditions and marine weather conditions in the Sea of Okhotsk in 2001 sea ice season (December 2000–May 2001). Proceedings of the 17th International Symposium on Okhotsk Sea & Sea Ice, Mombetsu, 123–127.

Kondo, J. (2000): Atmospheric Science near the Ground Surface. Tokyo, University of Tokyo Press, 324 p. (in Japanese).

Lange, M.A. and Eicken, H. (1991): Textural characteristics of sea ice and the major mechanism of ice growth in the Weddell Sea. Ann. Glaciol., **15**, 210–215.

Linke, R. (1942): Handbuch der Geophysik. VIII, Berlin-Zehleudorf, Verlag von Gebruder Borntaeger.

Morris, K. and Jeffries, M.O. (2001): Seasonal contrasts in snow-cover characteristics on Ross Sea ice floes. Ann. Glaciol., **33**, 61–68.

SeaSpace Corp. (1995): TeraScan 2.6 Reference Manual; Vol. 1, 328–331.

Shimoda, H., Endo, T., Muramoto, K., Ono, N., Takizawa, T., Ushio, S., Kawamura, T. and Ohshima, K. (1997): Observations of sea-ice conditions in the Antarctic coastal region using ship-board video cameras. Nankyoku Shiryô (Antarct. Rec.), **41**, 355–365 (in Japanese with English abstract).

Shine, K.P. (1984): Parameterization of the shortwave flux over high albedo surfaces as a function of cloud thickness and surface albedo. Q. J. R. Meteorol. Soc., **110**, 747–764.

Sturm, M., Morris, K. and Massom, R. (1998): The winter snow cover of the West Antarctic pack ice: its spatial and temporal variability. Antarctic Sea Ice: Physical Processes, Interactions and Variability, ed. by M.O. Jeffries. Washington, DC, American Geophysical Union, 1–18 (Antarct. Res. Ser., **74**).

Takizawa, T., Motoi, T., Motoyama, H., Yokoyama, E. and Ono, N. (1987): Layered structure of a pack ice off Mombetsu. Proceedings of the 2nd International Symposium on Okhotsk Sea & Sea Ice, Mombetsu, 10–11 (in Japanese).

Toyota, T. and Wakatsuchi, M. (2001): Characteristics of the surface heat budget during the ice-growth season in the southern Sea of Okhotsk. Ann. Glaciol., **33**, 230–236.

Toyota, T., Ukita, J., Ohshima, K.I., Wakatsuchi, M. and Muramoto, K. (1999): A measurement of sea ice albedo over the southwestern Okhotsk Sea. J. Meteorol. Soc. Jpn., **77**, 117–133.

Toyota, T., Kawamura, T. and Wakatsuchi, M. (2000): Heat budget in the ice cover of the southern Okhotsk Sea derived from in-situ observations. J. Meteorol. Soc. Jpn., **78**, 585–596.

Toyota, T., Kawamura, T. and Ukita, J. (2001a): Sea ice structure in the Sea of Okhotsk. Proceedings of the International Symposium on Atmosphere-Ocean-Cryosphere Interaction in the Sea of Okhotsk and the Surrounding Environment, Sapporo, 66–67.

Toyota, T., Kawamura, T. and Nakatsuka, T. (2001b): Contribution of snow to the sea ice growth in the southern Sea of Okhotsk. Proceedings of the International Symposium on Atmosphere-Ocean-Cryosphere Interaction in the Sea of Okhotsk and the Surrounding Environment, Sapporo, 56–57.

Tucker III, W.B., Grenfell, T.C., Onstott, R.G., Perovich, D.K., Gow, A.J., Shuchman, R.A. and Sutherland, L.L. (1991): Microwave and physical properties of sea ice in the winter marginal ice zone. J. Geophys. Res., **96**, 4573–4587.

Ukita, J., Kawamura, T., Tanaka, N., Toyota, T. and Wakatsuchi, M. (2000): Physical and stable isotopic properties and growth processes of sea ice collected in the southern Sea of Okhotsk. J. Geophys. Res., **105**, 22083–22093.

Worby, A.P., Jeffries, M.O., Weeks, W.F., Morris, K. and Jana, R. (1996): The thickness distribution of sea ice and snow cover during late winter in the Bellingshausen and Amundsen Seas, Antarctica. J. Geophys. Res., **101**, 28441–28455.

Yamamoto, G., Tanaka, M. and Arao, K. (1968): Hemispherical distribution of turbidity coefficient as estimated from direct solar radiation measurements. J. Meteorol. Soc. Jpn., **46**, 287–300.

Zillman, J.W. (1972): A study of some aspects of the radiation and heat budgets of the southern hemisphere oceans. Bureau of Meteorology, Australia, 562 p. (Meteorological Studies 26)

(Received March 29, 2002; Revised manuscript accepted July 4, 2002)